Measurement of Isoscalar Pair Correlation in ^{120}Sn Using (α, ^{6}Li) Probe*

Jia-Wei Cai (蔡佳伟)[1,2,3] Shinsuke Ota[2†] Masanori Dozono[4] Satoshi Adachi[5] Shutaro Hanai[6] Yuto Hijikata[4] Genki Hosoya[5] Nobu Imai[6] Masatoshi Itoh[5] Noritaka Kitamura[6] Shin'ichiro Michimasa[6] Takeshi Y. Saito[6,7] Xiao-Dong Tang (唐晓东)[1,3] Shumpei Yamazaki[5] Shohei Yonekura[5]

[1]Institute of Modern Physics, Chinese Academy of Sciences, Lanzhou 730000, China
[2]Research Center for Nuclear Physics, The University of Osaka, Osaka 567-0047, Japan
[3]School of Nuclear Science and Technology, University of Chinese Academy of Sciences, Beijing 100049, China
[4]Graduate School of Science, Kyoto University, Kyoto 606-8501, Japan
[5]Cyclotron and Radioisotope Center, Tohoku University, Sendai 980-8578, Japan
[6]Center for Nuclear Study, The University of Tokyo, Tokyo 113-003, Japan
[7]Atomic, Molecular and Optical Physics Laboratory, RIKEN, Saitama 351-0198, Japan

Abstract: Nucleon-pair correlations play a fundamental role in shaping nuclear structure. Two-nucleon transfer reactions provide a unique probe for investigating pair correlations in nuclei. A recent theoretical study has predicted significant proton-neutron (pn) pair correlations in the unconventional $N > Z$ region. To investigate isoscalar pn pair correlations, we measured the ^{120}Sn(α, ^{6}Li)^{118}In reaction in the laboratory angular range from 9° to 19°. Owing to the limited experimental energy resolution, no distinct peak corresponding to the ground state of ^{118}In was observed. By evaluating the low-excitation-energy region, an upper limit of the cross section for populating ^{118}In(g.s.) was extracted, yielding an integrated cross section of $\sigma = 0.42 \pm 0.02$ μb. The DWBA calculations for the transfer of a $\pi g_{9/2} \otimes \nu g_{7/2}$ pair using an assumed value of the two-nucleon amplitude (TNA) are consistent with the experimental cross section. The competition between simultaneous and sequential transfer in this heavy system was investigated. A comparison with the ^{120}Sn(α, ^{6}He)^{118}Sn reaction indicates that the pn pair-correlation strength is far weaker than that for neutron-neutron pair condensation.

Keywords: Transfer Reaction, Nuclear Pair Correlation, Nuclear Structure, DWBA

DOI: 10.1088/1674-1137/ae740a **CSTR:**

I. INTRODUCTION

Nucleon-pair correlations have long been one of the most compelling topics in nuclear physics [1−3]. In a relative S-wave, proton-neutron (pn) pairs may form in either the isovector ($T = 1$, $S = 0$) or the isoscalar (deuteronlike $T = 0$, $S = 1$) channel. The isoscalar pair condensate was initially predicted to become favorable in heavy $N = Z$ nuclei [4, 5]. More recently, such condensation was also predicted in heavy $N \approx Z$ nuclei along the proton-drip line [6]. Recently, Yoshida [7] calculated pn pair correlations in Sn isotopes within a framework utilizing the static pair polarizability (energy-inverse-weighted sum of pair transition strengths) [8] to quantify pair correlations. It was found that the isoscalar pair-removal strength peaks at ^{114}Sn ($N = 64$) and gradually declines starting from ^{116}Sn. This study is directly relevant to pair-removal measurements aimed at extracting the pairing strength.

The two-nucleon transfer reaction is a unique tool for probing nucleon-pair correlations in many-body systems, as the reaction cross section can be enhanced by pair correlations [9, 10] relative to the transfer of uncorrelated nucleons. The nn pair condensation has been well established using (p, t) and (t, p) reactions on tin isotopes [11, 12], whereas clear evidence for the condensation of pn pairs remains elusive. Traditionally, research on pn pairing has focused on the $N = Z$ region. The (p, ^{3}He) and (^{3}He, p) reactions have been employed to study the transfer of two types of pn pairs [13], and second-order DWBA calculations have been applied to pn transfer for the first time. The experimental study of the radioactive self-conjugate fp-shell nuclei ^{56}Ni and ^{52}Fe [14] shows no evidence for a $T = 0$ pn condensate. Recent predictions of pn pair correlations in $N > Z$ nuclei challenge the

Received 31 March 2026; Accepted 28 May 2026

* This work was supported by JSPS KAKENHI (No. 19H05143, 20H01928 and 25H00640). J. Cai acknowledges support from the National Key Research and Development program (MOST 2022YFA1602304) and the National Natural Science Foundation of China (No. 12335009). The research also received funding from the Chinese Scholarship Council (No. 202204910371)

† E-mail: Corresponding author: ota@rcnp.osaka-u.ac.jp

long-held notion that such pairing exists predominantly in $N = Z$ nuclei, thereby extending the study of *pn* pairs into the neutron-rich regime [6, 7]. The unique capability of (d, α) and (α, ^{6}Li) transfer reactions lies in their spin-isospin selectivity, which ensures that only the isoscalar *pn* pair component can be identified. In a recent measurement of the (d, α) reaction on the neutron-rich ^{138}Ba ($N = 82$) nucleus [15], the cross-section angular distribution was reproduced within the distorted-wave Born-approximation (DWBA) framework by assuming transfer of a deuteron (d) cluster.

We revisited the (α, ^{6}Li) reaction and its potential for investigating nucleon-pair correlations in neutron-rich nuclei. This probe has previously been employed to study d and α clustering in light and intermediate $N = Z$ nuclei [16–20], populating not only ground states but also excited states of the residual nuclei. To experimentally access the static pair polarizability [7, 8], the pairing strength over a wide excitation-energy range, from the ground state to the 20 – 30 MeV excitation-energy region, should be extracted via multipole decomposition analysis using the angular distributions of pair-transfer reactions. The momentum matching for the ^{120}Sn(α, ^{6}Li) reaction at incident energies of ~ 20 MeV/A indicates that low-angular-momentum transfer would be enhanced.

Tin isotopes, with the magic number $Z = 50$, have been confirmed as neutron superfluid systems [1]. The outermost proton of ^{120}Sn occupies the intruder $1g_{9/2}$ orbital; consequently, the ground states of known even-N indium isotopes exhibit a spin–parity of $9/2^+$, reflecting the presence of a proton hole. The odd-odd nucleus ^{118}In, whose ground state is 1^+, is β^--unstable and can decay into the ground state of ^{118}Sn via a Gamow–Teller transition predominantly involving the $\pi 1g_{9/2}$ and $\nu 1g_{7/2}$ orbitals. The configuration of $\pi 1g_{9/2}^{-1} \otimes \nu 1g_{7/2}^{-1}$ has been used to describe the ^{118}In ground-state wave function [21]. These two orbitals reside in different major shells due to the spin-orbit interaction [22], but the substantial overlap of their radial wave functions may give rise to a strong *pn* interaction [23], facilitating the formation of an isoscalar $\pi 1g_{9/2} \otimes \nu 1g_{7/2}$ pair and enhancing the pair-transfer probability. This configuration also precludes the formation of an isovector *pn* pair, thereby rendering the reaction exclusively sensitive to isoscalar pairing.

This work represents the first measurement of the (α, ^{6}Li) reaction on a ^{120}Sn target, aimed at investigating the transition to the ground state of ^{118}In. The upper limit of the experimental cross section for population of the ^{118}In ground state was determined and compared with calculations within the DWBA framework. The interplay between simultaneous and sequential *pn* pair transfer was investigated. The ^{120}Sn(α, ^{6}He)^{118}Sn reaction was also measured to serve as a reference for evaluating the isoscalar *pn* pair-correlation strength.

II. EXPERIMENT

The experiment was conducted at the Cyclotron and Radioisotope Center (CYRIC), Tohoku University, using a ^{120}Sn target with a thickness of 3.6 mg/cm^2. An α beam with an intensity of approximately 3 nA, accelerated by the K110 AVF cyclotron, was directed onto the target in the scattering chamber. A schematic diagram of the experimental setup is shown in Fig. 1. The ejectiles, after passing through a Mylar degrader, were detected by an array of three silicon detectors backed by a plastic scintillator, which served as a veto detector to reject elastically scattered α particles. The detector array was centered at 13.4° with respect to the beam direction, covering an angular range from 9° to 19° in the laboratory frame. An identical array was installed symmetrically on the opposite side of the beamline to improve statistics. Two dipole magnets positioned upstream of the scattering chamber ensured a beam energy of 100 MeV. A Faraday cup placed downstream was used to monitor the beam intensity.

Three silicon detectors enabled particle identification (PID) using the $\Delta E - E$ technique. Arranged in the order traversed by the particles, the thicknesses of the three silicon detectors were 140,500, and 1500 μm, respectively. The second detector was a double-sided silicon strip detector (DSSSD), which allowed the extraction of angular information. To maintain a low dead time in the data acquisition system, the silicon detectors were partially masked to reduce the event rate at forward angles, where the counting rate was dominated by elastic scattering.

The dead-layer thicknesses of the silicon detectors were specified as 0.5 μm in the detector manual and were verified using an α source on the DSSSD. The energy loss of the particles in these dead layers, particularly for heavy ejectiles, was calculated using the stopping powers provided by the SRIM code [24]. Owing to the limitations of our experimental setup, it was not possible to resolve the low-lying states in the high-level-density excitation spectrum of ^{118}In; therefore, a Kapton target was also mounted on the target ladder to ensure reliable energy

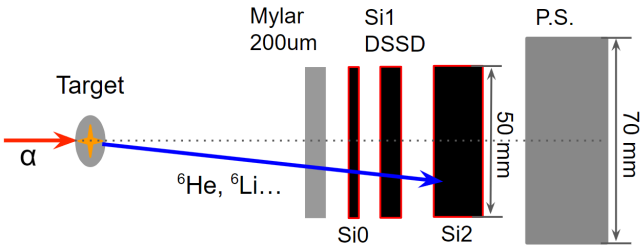

Fig. 1. (color online) Side view of a detector array in the experimental setup. The red borders schematically indicate the dead layers of the silicon detectors. Both arrays were masked at forward angles to reduce the number of elastic events and the event rate.

calibration of the silicon detectors using the reactions between the beam and the carbon in the target. The linearity of the MSCF-16 shaping amplifier and the MADC-32 analog-to-digital converter was checked using a pulser for each silicon detector.

III. DATA ANALYSIS

A. Energy Calibration

The PID procedure was used to select ^{6}He and ^{6,7}Li events. The collected charge was calibrated using a triple-α source and a Kapton target. The ^{12}C(α, ^{7}Li)^{9}B reaction was used to calibrate the energy deposited by heavier particles in the first two silicon detectors, because its excitation spectrum consists of well-separated levels. The 3.35 MeV state of ^{10}C populated via the ^{12}C(α, ^{6}He)^{10}C reaction was used to calibrate the last silicon detector. The resulting parameters were then applied to the ^{6}Li ejectiles from the Kapton and ^{120}Sn targets. The correlation between the energy deposited in the sensitive volume of Si_0, denoted E_{Si0}, and the sum of the energies deposited in Si_{1x} and Si_2, $E_{Si1x}+E_{Si2}$, is depicted in Fig. 2. A clear separation of particle species is observed, and the ^{6}Li events of interest are successfully identified and isolated.

The energy loss in the Mylar degrader was calculated. The effect of the uncertainty in the stopping powers provided by the SRIM code [24] on the total kinetic energy of the ejectiles, and consequently on the deduced excitation energy, was also evaluated. As shown in Fig. 3, although the first excited state is not fully resolved from the ground-state data, the centroids of the excitation energies of the ground state and two excited states of the ^{12}C(α, ^{6}Li)^{10}B reaction were found to be well within 50 keV of their nominal values. This confirms the reliability of the energy calibration and the consistency of the stopping-power calculations across different lithium isotopes. The accuracy of the SRIM code for helium and lithium was further assessed by scaling the stopping powers within their reported uncertainties [24]. The energies of the ^{7}Li and ^{6}He particles were well reproduced, and the deviations for the low-lying states in the (α, ^{6}Li) reaction were found to be well within 200 keV. The energy calibrations for the two detector arrays were in good agreement; for both the (α, ^{6}Li) and (α, ^{7}Li) channels, the observed differences were within 100 keV. This confirms the consistency between the left and right arrays.

The emission angle of each ejectile was determined using the DSSSD. In the analysis of elastic scattering, the orientation of the detector array relative to the beam direction was observed to vary slowly within a small range, reflecting fluctuations in the beam incidence angle and variations in the beam spot position on the target. These variations remained within the width of a single DSSSD

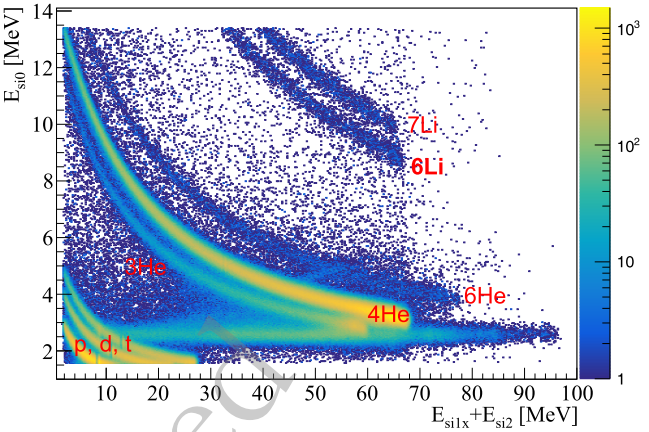

Fig. 2. (color online) PID correlation for ejectiles from the ^{120}Sn target. The horizontal axis represents the energies deposited in the last two silicon detectors, and the vertical axis represents the energy deposited in the first silicon detector. From the lower left to the upper right: p, d, t, ^{3,4,6}He, and ^{6,7}Li.

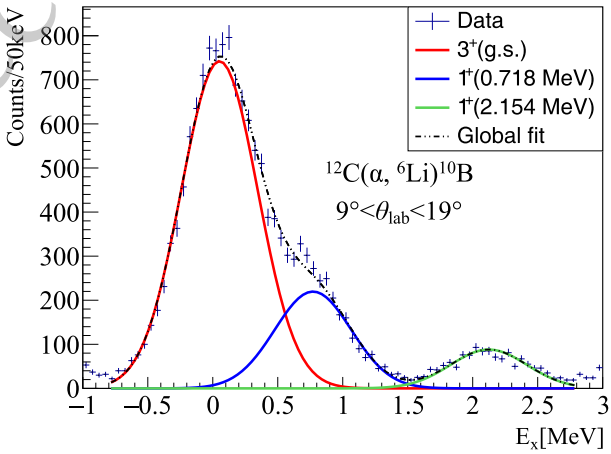

Fig. 3. (color online) Excitation-energy spectrum for the ^{12}C(α, ^{6}Li)^{10}B reaction. The ground state and excited states were fitted with the red, blue, and green curves, respectively. The black curve represents the global fit.

pixel, resulting in an angular uncertainty of 0.6°. The fraction of events with multiplicity (i.e., events in which more than one hit was recorded in a single silicon pad) was approximately 0.3% of the total number of events. The dominant contribution to the overall multiplicity arose from the DSSSD strip pitch, with a multiplicity rate of about 3.4% on the Ohmic side and a similar value on the junction side. Event pile-up was found to be negligible. In total, an estimated correction of approximately 8% should be applied to the measured cross section. Elastic scattering from the Kapton target was also analyzed. The angular distribution of elastic counts in the laboratory frame was found to be in good agreement with calculations based on optical model potentials (OMPs) taken from Ref. [25], thereby validating the reliability of the data analysis procedure.

B. Excitation Spectrum

The excitation-energy spectrum of the residual nucleus ^{118}In is shown in Fig. 4. It exhibits a quasi-continuous structure due to the limited experimental energy resolution and the high level density of ^{118}In (nine known states below 0.5 MeV [26], including, in particular, the 60 keV (5^+) isomeric state), preventing the extraction of discrete transition strengths. Under these conditions, a precise evaluation of the energy resolution and the uncertainty in the energy calibration becomes essential for reliably analyzing the transfer to the ground state. The uncertainty in the energy calibration was checked in Sec. III A, and excellent consistency was achieved.

The overall energy resolution (FWHM) of the ^{120}Sn(α, ^{6}Li)^{118}In(g.s.) reaction was calculated to be 450 keV, taking into account the energy-loss distribution of outgoing ^{6}Li particles in the target and the energy straggling in the degrader. The excitation-energy resolutions obtained for the ^{12}C(α, ^{6,7}Li) channels using the same procedure were found to be in excellent agreement with the experimentally extracted values, indicating that the contribution from electronics is negligible.

The nitrogen in Kapton gives rise to ^{6}Li particles originating from the ^{14}N(α, ^{6}Li)^{12}C(4.44 MeV) reaction, whose energies are nearly identical to those from the ^{120}Sn(α, ^{6}Li)^{118}In(g.s.) reaction. Therefore, this ^{12}C state is of great importance for evaluating the shift of the ground-state centroid in the excitation spectrum of ^{118}In. The analysis shows that the centroid of the 4.44 MeV state of ^{12}C shifts to higher energy by 0.12 MeV relative to its actual energy. This shift is well within the range of the deviation calculated in Sec. III A, leading to the conclusion that the most probable excitation-energy centroid of the ground state is 0.12 MeV, as schematically shown by the red Gaussian in Fig. 4. The effect of the angle uncertainty in Sec. III A on the energy was also considered. This uncertainty can induce a small kinematic energy difference, resulting in an excitation-energy uncertainty of less than 0.03 MeV, which is much smaller than 0.12 MeV.

In the following analysis, the centroid of the ^{118}In ground state in Fig. 4 was taken to be 0.12 MeV. Under the assumption that the excitation-energy distribution of the ^{118}In ground state has a Gaussian form, events with $E_x < 0.12$ MeV were attributed to the ground-state events, and their count was multiplied by a factor of two in the process of obtaining the cross section. This approach unavoidably includes contributions from excited states and thus can only serve as an upper limit of the transfer cross section.

C. Angular Distribution

The analysis of the pair transfer reaction ^{120}Sn(α, ^{6}Li)^{118}In(g.s.) yields an upper limit (UL) on the cross section of the ground-state transition. As shown by the black

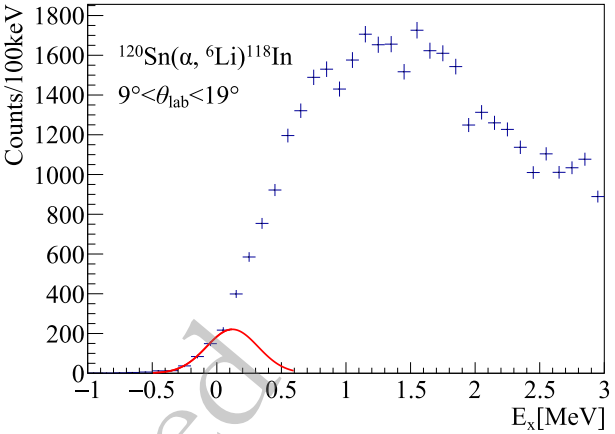

Fig. 4. (color online) Excitation-energy spectrum of the ^{120}Sn(α, ^{6}Li)^{118}In reaction. The red curve indicates the upper limit of the ground-state event distribution.

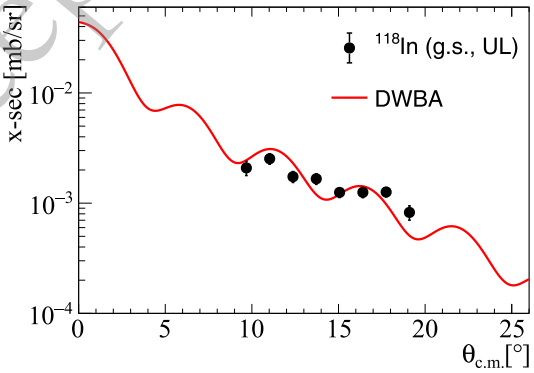

Fig. 5. (color online) Experimentally deduced upper limits (ULs) on the differential cross sections for the ^{120}Sn(α, ^{6}Li)^{118}In(g.s.) reaction. The red curve shows the calculated total cross section within the second-order DWBA framework, including both the ^{5}He+^{119}Sn and ^{5}Li+^{119}In intermediate paths (see text for details). The experimental resolution was folded into the calculations.

solid circles in Fig. 5, the experimental result exhibits a gradually decreasing trend, and two weak oscillatory features are observed, with maxima at $\theta_{cm} = 11°$ and 18°. The statistical uncertainties exceed the systematic ones, and at certain angles the error bars in the distribution are smaller than the symbol size. The differential cross section is less than 3 μb/sr at forward angles, and the integrated cross section within the measured angular range was determined to be 0.42 ± 0.02 μb.

1. *DWBA pn pair transfer*

To fully understand the underlying reaction mechanism, second-order DWBA calculations including both simultaneous and sequential transfer of two non-identical nucleons were performed. Unlike the two-neutron transfer reaction, sequential *pn* transfer can proceed through two distinct paths: the intermediate partition ^{5}Li+^{119}In

populated via proton transfer, and ^{5}He+^{119}Sn populated via neutron transfer. In both cases, the intermediate nuclei (^{5}Li and ^{5}He) are unbound. The following calculations were therefore performed under the assumption that the transfer process occurs prior to their decay. The finite-range *prior-post* representation [13, 27] was adopted for the sequential transfer in order to avoid the non-orthogonality term [27]. Calculations were carried out using the computer code FRESCO [28].

The OMPs describing elastic scattering of the reactants in the entrance and exit channels were taken from Hauser et al. [25] and Huffman et al. [29], respectively. Due to the absence of available OMPs for the core-core interactions, the OMP for α-scattering was employed. The single-particle wave functions of the transferred nucleons in ^{6}Li were constructed using a Woods–Saxon potential with parameters $r_0 = 1.25$ fm and $a = 0.65$ fm for each path. The binding energy was set to half of the Q-value for separating a proton and a neutron from ^{6}Li [30, 31], and the depths were adjusted to reproduce the energies. For the single-particle states in ^{120}Sn, the same parameters were used. In the intermediate partitions, the ^{119}In$(9/2^{+})$ and ^{119}Sn$(7/2^{+})$ states were included based on the prediction in Ref. [7]. These wave functions were also adopted in the simultaneous calculation.

The two-nucleon amplitudes (TNAs) associated with the nuclear overlaps of the aforementioned ^{6}Li single-particle states were calculated using the KSHELL [32] code within the *psd*-shell model space and the YSOX effective interaction [33]. The dominant contributions were found to arise from the $1p_{1/2}$ and $1p_{3/2}$ orbitals. For ^{120}Sn, the number of nucleons outside the doubly magic ^{100}Sn core is 20. The large model space, together with the proton hole in ^{118}In, makes reliable shell-model calculations challenging. According to Ref. [7], the $\nu 1g_{7/2}$ orbital and its intruder partner $\pi 1g_{9/2}$ dominate the isoscalar pairing correlation. Therefore, a TNA value of 0.75 was adopted for the $\pi g_{9/2} \otimes \nu g_{7/2}$ pair removal, which enables the DWBA calculations to reproduce the experimental data. For the spectroscopic amplitudes associated with the overlap functions in the sequential transfer, the TNAs were decomposed into two components through the intermediate states following the prescription of Ref. [13].

The calculated full transfer cross section via both intermediate partitions is presented in Fig. 5. For the simultaneous process, the *post*-form with complex remnant terms of the potential [28] was adopted. The calculated angular distributions were folded with the experimental angular resolution. The red curve represents the coherent sum of the simultaneous and two sequential transfer processes. In this calculation, the two-nucleon wave functions for the simultaneous process were constructed from the single-particle states for the ^{5}He+^{119}Sn sequential path. The calculation exhibits a strongly forward-peaked angular distribution with regular oscillatory behavior for the population of the ground state in ^{118}In. An additional calculation performed using the same procedure, but with wave functions constructed from the ^{5}Li+^{119}In path, yields nearly identical cross sections to those shown in Fig. 5. This indicates that the full calculation depends only weakly on the choice of the single-particle states. Both calculations are reasonably consistent with the experimental upper limit for the ground-state transition when using an input TNA value of 0.75.

The individual contributions from the simultaneous direct *pn*-pair transfer and the two competing sequential processes are presented together with the complete calculation in Fig. 6. The effect of the experimental angular resolution was not included. The decomposition of the sequential transfer into the two intermediate paths shows that the ^{5}Li+^{119}In route plays a more dominant role in the sequential cross section than the ^{5}He+^{119}Sn route, contributing by more than a factor of two. This difference may be attributed to the involvement of different single-particle configurations in ^{120}Sn associated with the distinct spins of the intermediate states. The total sequential-transfer contribution (full blue curve) is larger than that from the simultaneous process, with the latter exhibiting large-amplitude oscillatory behavior. This indicates that the transferred *pn* system is not sufficiently correlated for the simultaneous transfer to dominate over the transfer of two uncorrelated nucleons. The phase coherence [34] between the simultaneous and sequential amplitudes was found to be weak. We therefore conclude that the use of an assumed TNA value does not affect the discussion of the reaction mechanism, owing to the relation between the spectroscopic amplitudes associated with the simultaneous and sequential processes [13].

The results obtained in the *prior* form for simultan-

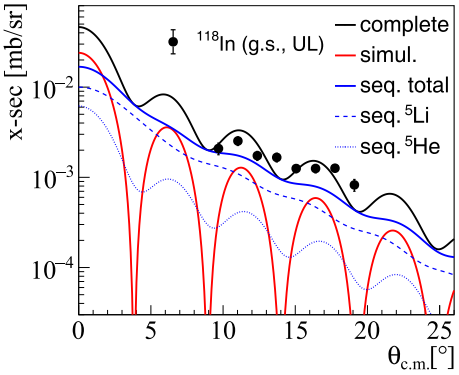

Fig. 6. (color online) Calculated angular differential cross sections for the ^{120}Sn(α, ^{6}Li)^{118}In(g.s.) reaction proceeding through different transfer mechanisms. The black curve represents the coherently summed total cross section. The red (blue) curve corresponds to simultaneous (sequential) transfer. The dashed and dotted blue curves denote sequential transfer through the ^{5}Li and ^{5}He intermediate partitions, respectively. The experimental angular resolution was not included.

eous transfer show only minor differences from those presented in Fig. 6, indicating good consistency between the *prior*- and *post*-form Hamiltonians for this system. It is worth noting that global phenomenological OMPs for the α [35] and ^{6}Li [36] channels were also employed in the calculations. The resulting changes were negligible and did not affect the overall conclusions, demonstrating that the calculations are not particularly sensitive to the choice of OMPs.

2. *Deuteron cluster transfer*

Cluster degrees of freedom have long been an important topic in nuclear physics [37]. Interest in this field has recently been renewed by efforts to investigate cluster structures in the ground states of heavy nuclei, such as tin isotopes, using quasi-free cluster knockout reactions [38–40]. The spectroscopic factors (SFs) extracted from knockout reactions have been compared with those obtained from transfer reactions over a wide mass range [41], because both processes probe essentially the same underlying nuclear structure information.

The $d+\alpha$ cluster structure of ^{6}Li is well established [42–44] and has been extensively exploited in studies of cluster formation via transfer reactions [16, 17]. We performed DWBA calculations assuming a direct pickup mechanism, in which a neutron in the $\nu 1g_{7/2}$ orbital and a proton in the $\pi 1g_{9/2}$ orbital are transferred as an inert cluster [11, 12, 15, 19]. As pointed out in Ref. [41], the extracted SFs depend on the OMPs and overlap functions. Therefore, all four combinations of the OMPs employed in the pair-transfer calculations were adopted in the present calculations. The number of nodes N and the orbital angular momentum L of the cluster wave function relative to the core were determined according to the conservation rule for harmonic-oscillator quanta [45]. For the unnatural-parity 1^+ state, transfers with $J=L\pm1$ are allowed, as listed in Table 1. The radius of the $d+\alpha$ binding potential was taken to be 1.9 fm [42] when generating the wave function. The spectroscopic factor $S_{d+\alpha}$ for the $^6\mathrm{Li}\rightarrow d+\alpha$ overlap was fixed at unity [46, 47]. The geometry of the $d+^{118}$In potential was chosen to be identical to that adopted in Sec. III C 1.

The DWBA calculations performed using the OMPs from Refs. [25, 29], shown in Fig. 7, were convoluted with the experimental angular resolution. The transfer of a deuteron in the $5S$ configuration relative to ^{118}In is represented by the red curve, which similarly exhibits the forward-angle peaking behavior observed in Fig. 5. The calculated cross section was normalized to the experimental upper limit to determine the spectroscopic factor.

$$S_{d+^{118}In}=\frac{\mathrm{d}\sigma_{exp}}{\mathrm{d}\Omega}\Big/\frac{\mathrm{d}\sigma_{\mathrm{DWBA}}}{\mathrm{d}\Omega}.$$

Table 1. The upper bound on the d-spectroscopic factor. The $5S$ and $4D$ states correspond to d-cluster states relative to the core.

State	L	$S_{d+^{118}\mathrm{In}}$
$5S$	0	$0.68\pm0.02_{stat}\pm0.05_{sys}$
$4D$	2	$0.90\pm0.02_{stat}\pm0.13_{sys}$

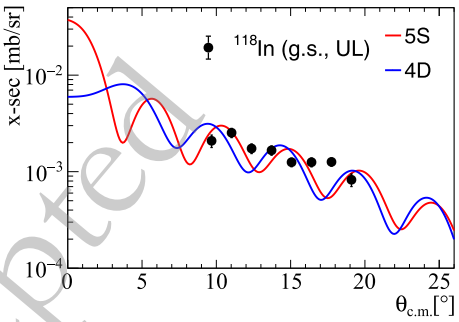

Fig. 7. (color online) The upper limit (UL) of the differential cross section for ^{120}Sn(α, ^{6}Li)^{118}In(g.s.) is shown. The red curve shows calculations for the d cluster in the $5S$ state relative to the core. The blue curve shows results for the d cluster in the $4D$ state.

The calculations performed using different combinations of OMPs [35, 36] yield comparable angular distributions and absolute strengths, indicating weak sensitivity to the choice of OMPs. Taking the small variations among these calculations into account gives a final upper-limit value for the spectroscopic factor, summarized in Table 1, of $S_{d+^{118}\mathrm{In}}=0.68\pm0.02_{stat}\pm0.05_{sys}$, under the assumption that the ground-state transition exhausts the full transfer strength. 0.02_{stat} denotes the statistical uncertainty, while 0.05_{sys} represents the systematic uncertainty associated with the different choices of OMPs.

The calculation for the $4D$ configuration is shown as the blue curve in Fig. 7. In contrast to the $5S$ component, the forward-angle peaking behavior disappears. The extracted spectroscopic factor is $S_{d+^{118}\mathrm{In}}=0.90\pm0.02_{stat}\pm0.13_{sys}$. As evident from Fig. 7, measurements at forward angles are crucial for quantitatively determining the relative contributions of the two configurations and, consequently, for obtaining a more reliable experimental constraint on the spectroscopic factors.

3. *(α, ^{6}He) reaction*

The ground states of the even-N tin isotopes are well known to exhibit neutron-superfluid character [1]. In the present work, the (α, ^{6}He) channel was also investigated, since strong nn pairing correlations are expected to enhance the transfer to the ground state of ^{118}Sn [11, 12] relative to the transfer of two weakly correlated neutrons. In contrast to the ^{6}Li channel, the excitation spectrum observed in the ^{6}He channel exhibits well-resolved struc-

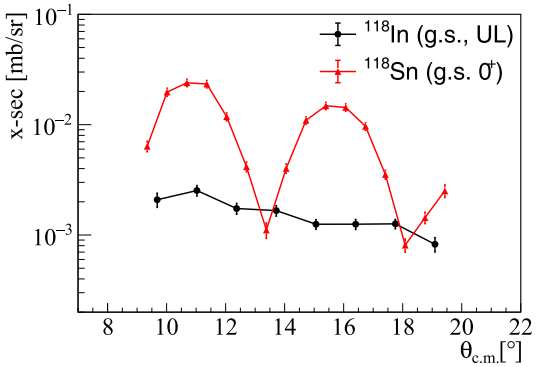

Fig. 8. (color online) The experimental angular differential cross sections are shown. Red triangles represent the ^{120}Sn(α, ^{6}He)^{118}Sn(g.s.) transition. Black circles denote the upper limit (UL) for the ^{120}Sn(α, ^{6}Li)^{118}In(g.s.) reaction. The lines connecting the data points are drawn to guide the eye.

tures, allowing the ground state of ^{118}Sn to be clearly identified. The angular distribution of the differential cross section is shown by the red triangles in Fig. 8. Two pronounced oscillatory maxima were observed at $\theta_{cm} \sim 11°$ and 16°. The first peak reaches approximately 0.02 mb/sr, more than an order of magnitude larger than the upper limit deduced for the ground-state transition to ^{118}In, shown by the black solid circles.

The ^{120}Sn(α, ^{6}Li)^{118}In and ^{120}Sn(α, ^{6}He)^{118}Sn reactions were measured under identical experimental conditions to minimize systematic uncertainties. The two reactions have very similar Q values and momentum-matching conditions; therefore, kinematic effects are expected to make a negligible contribution to the difference between the two cross sections shown in Fig. 8. The *nn* transfer between even-A tin isotopes is strongly enhanced owing to the condensate-like nature of the neutron pairs, providing a useful benchmark for investigating the strength of the *pn* pairing correlation. The angular differential cross section for the transition to ^{118}In(g.s.) is approximately one order of magnitude smaller than that for the transition to ^{118}Sn(g.s.), indicating that the isoscalar *pn* pairing correlation in ^{120}Sn is substantially weaker than the corresponding *nn* pairing correlation. It can therefore be concluded that the isoscalar *pn* pairing correlation is not significant compared with the strong *nn* pair condensation observed in the tin isotopes. A detailed investigation of the ^{120}Sn(α, ^{6}He)^{118}Sn reaction over a wide excitation-energy range is in preparation [48] and will be reported in a forthcoming publication.

IV. CONCLUSION AND OUTLOOK

The ^{120}Sn(α, ^{6}Li)^{118}In reaction was measured for the first time at $E_{\alpha} = 100$ MeV over the angular range $\theta_{lab} = 9°–19°$. The spin-isospin selectivity of the (α, ^{6}Li) probe enabled us to focus specifically on the isoscalar *pn* pairing correlation in the heavy neutron-rich singly closed-shell nucleus ^{120}Sn. A reliable energy calibration for the detected ^{6}Li particles was achieved through the analysis of several reaction channels induced on a Kapton target. However, the finite energy resolution of the experimental setup broadened the excitation-energy spectrum of ^{118}In, preventing a precise extraction of the strength of the isoscalar pairing correlation.

In this work, the low-excitation region of ^{118}In was investigated. An upper limit for the cross section populating the 1^{+} ground state was evaluated. The forward-angle differential cross section was found to be less than 3 μb/sr, while the integrated cross section over the measured angular range was determined to be 0.42 ± 0.02 μb. Second-order DWBA calculations including both the ^{5}Li+^{119}In and ^{5}He+^{119}Sn routes were found to be consistent with the experimental data. A TNA value for the $\pi 1g_{9/2} \otimes \nu 1g_{7/2}$ pair configuration removed from ^{120}Sn was adopted following the prediction of Ref. [7]. The competition between simultaneous and sequential mechanisms was investigated in detail. The calculations show that the sequential process dominates the transfer, indicating that the isoscalar *pn* pairing mode is not strongly enhanced. Cluster-transfer calculations were also performed, and upper limits for the deuteron spectroscopic factors were extracted. The results indicate that both DWBA calculations are only weakly sensitive to the choice of OMPs. The ^{120}Sn(α, ^{6}He)^{118}Sn reaction was additionally measured and compared with the ^{6}Li channel. The observed difference of approximately one order of magnitude in the cross sections indicates that the isoscalar *pn* pairing correlation is substantially weaker than the corresponding *nn* pairing correlation in this neutron-rich system.

The investigation of *pn* pairing correlations remains an ongoing topic within the PHANES collaboration, as their underlying nature is not yet fully understood. Unlike the conventional (p, ^{3}He) approach, the isoscalar and isovector pairing strengths can be selectively probed through an appropriate choice of reaction probes, such as (d, α) and (α, ^{6}Li). Neutron-rich nuclei are not the sole focus of this project; self-conjugate nuclei are also planned for investigation, since they provide important reference systems for comparison. To systematically study the mass dependence of the *pn* pairing correlations [7], pair-removal responses along isotopic chains will be investigated. As a next step, forward-angle measurements for both neutron-rich and self-conjugate nuclei have been proposed using the magnetic spectrometers at RCNP.

ACKNOWLEDGMENTS

The authors thank M. Matsuo, S. Shimoura, K. Yoshida and S. S. Perrotta for insightful discussions, as well as the other members of the PHANES Collaboration. We appreciate the CYRIC cyclotron staff for high-quality beam.

References

[1] D. Brink and R. A. Broglia, *Nuclear Superfluidity: Pairing in Finite Systems* (Cambridge University Press, Cambridge, 2005).
[2] D. J. Dean and M. Hjorth-Jensen, Rev. Mod. Phys. **75**, 607 (2003)
[3] S. Frauendorf and A. Macchiavelli, Prog. Part. Nucl. Phys. **78**, 24 (2014)
[4] A. Goswami and L. S. Kisslinger, Phys. Rev. **140**, B26 (1965)
[5] K. Yoshida, Phys. Rev. C **90**, 031303 (2014)
[6] A. Gezerlis, G. F. Bertsch, and Y. L. Luo, Phys. Rev. Lett. **106**, 252502 (2011)
[7] K. Yoshida, Proton-neutron pair correlations in neutronrich nuclei (2024), arXiv: 2411.13963[nucl-th].
[8] K. Takahashi, Y. Matsuda, and M. Matsuo, Prog. Theo. Exp. Phys. **2023**, 083D01 (2023)
[9] S. Yoshida, Nucl. Phys. **33**, 685 (1962)
[10] P. Fröbrich, Phys. Lett. B **37**, 338 (1971)
[11] P. Guazzoni, L. Zetta, A. Covello, *et al*., Phys. Rev. C **78**, 064608 (2008)
[12] P. Guazzoni, M. Jaskola, L. Zetta, *et al*., Phys. Rev. C **60**, 054603 (1999)
[13] Y. Ayyad, J. Lee, A. Tamii, *et al*., Phys. Rev. C **96**, 021303 (2017)
[14] B. Le Crom, M. Assié, Y. Blumenfeld, *et al*., Phys. Lett. B **829**, 137057 (2022)
[15] B. M. Rebeiro, S. Triambak, P. E. Garrett, *et al*., Phys. Rev. Lett. **131**, 052501 (2023)
[16] G. Fazio, G. Giardina, O. Y. Goryunov, *et al*., J. Phys. Soc. Jpn **64**, 1141 (1995)
[17] B. Zeidman, H. T. Fortune, and A. Richter, Phys. Rev. C **2**, 1612 (1970)
[18] C. D. Zafiratos, Phys. Rev. **136**, B1279 (1964)
[19] R. G. Markham and M. A. M. Shahabuddin, Phys. Rev. C **14**, 2037 (1976)
[20] L. G lowacka, J. Turkiewicz, and O. Goryunov, Nucl. Phys. A **534**, 349 (1991)
[21] D. D. Frenne, H. Thierens, E. Jacobs, *et al*., Phys. Rev. C **15**, 1440 (1977)
[22] A. Martinou, D. Bonatsos, N. Minkov, *et al*., Eur. Phys. J. A 56, 10.1140/epja/s10050-020-00239-0 (2020).
[23] C. Babcock, R. Klawitter, E. Leistenschneider, *et al*., Phys. Rev. C **97**, 024312 (2018)
[24] J. F. Ziegler, M. Ziegler, and J. Biersack, Nucl Instrum. Meth. B **268**, 1818 (2010)
[25] G. Hauser, R. Löhken, H. Rebel, *et al*., Nucl. Phys. A **128**, 81 (1969)
[26] National Nuclear Data Center, https://www.nndc.bnl.gov/nudat3, accessed: 2026-01-15.
[27] T. Udagawa, H. H. Wolter, and W. R. Coker, Phys. Rev. Lett. **31**, 1507 (1973)
[28] I. J. Thompson, Comp. Phys. Rep. **7**, 167 (1988)
[29] R. Huffman, A. Galonsky, R. Markham, *et al*., Phys. Rev. C **22**, 1522 (1980)
[30] J. C. Zamora, J. L. Ferreira, A. Barioni, *et al*., Phys. Rev. C **106**, 014603 (2022)
[31] S. S. Perrotta, M. Colonna, and J. A. Lay, Phys. Rev. C **108**, 044614 (2023)
[32] N. Shimizu, T. Mizusaki, Y. Utsuno, *et al*., Comput. Phys. Commun. **244**, 372 (2019)
[33] C. Yuan, T. Suzuki, T. Otsuka, *et al*., Phys. Rev. C **85**, 064324 (2012)
[34] I. J. Thompson, Reaction mechanisms of pair transfer, in *Fifty Years of Nuclear BCS* (World Scientific, 2013) p. 455–467.
[35] M. Nolte, H. Machner, and J. Bojowald, Phys. Rev. C **36**, 1312 (1987)
[36] Y. Xu1, Y. Han, J. Hu, *et al*., Phys. Rev. C **98**, 024619 (2018)
[37] K. Ikeda, N. Takigawa, and H. Horiuchi, Prog. Theo. Phys. Suppl. **E68**, 464 (1968)
[38] J. Tanaka, Z. Yang, and S. Typel, Science **371**, 260 (2021)
[39] Y. Kubota, K. Agbekponou, D. Ahn, *et al*., Nucl. Phys. A **1060**, 123123 (2025)
[40] J. Tanaka, T. Uesaka, J. Zenihiro, *et al*., RCNP Annual Report 2024 (2024)
[41] T. A. Carey, P. G. Roos, N. S. Chant, *et al*., Phys. Rev. C **29**, 1273 (1984)
[42] H. Nishioka, J. Tostevin, R. Johnson, *et al*., Nucl. Phys. A **415**, 230 (1984)
[43] A. T. Rudchik, A. A. Rudchik, O. O. Chepurnov, *et al*., Phys. Rev. C **103**, 044614 (2021)
[44] K.-I. Kubo and M. Hirata, Nucl. Phys. A **187**, 186 (1972)
[45] I. Talmi, *Nuclear spectroscopy with harmonic oscillator wave-functions*, Ph.D. thesis, ETH Zurich (1952).
[46] N. Keeley, K. Kemper, and D. T. Khoa, Nucl. Phys. A **726**, 159 (2003)
[47] B. Zhou and D. Tao, Private communications, Fudan University, 2025-05-25.
[48] M. Dozono, Measurement of highly-excited neutron-pair vibration, Microscopic approach from pair correlation to pair condensation (2024), accessed: 2025-05-29.